Research on Engineering Structures & Materials
www.jresm.org
MIM Research Group

Research Article

Effect of geogrid reinforcement location on the structural performance of flexible pavements under full-scale accelerated loading

Ahmed Fahim Rahi [*,a], Ali Majeed Al-Dahawi [b], Ahmed Subhi Abduljabbar [c]

College of Civil Engineering, University of Technology, Baghdad, Iraq

Article Info

Article History:

Received 19 May 2025

Accepted 23 July 2026

Keywords:

Geogrid reinforcement;
Flexible pavement;
Accelerated pavement testing;
Rutting;
Subgrade stress;
Tensile strain

Abstract

Geogrid reinforcement is widely used to improve flexible pavements over weak subgrades, yet full-scale evidence on the effect of reinforcement location under repeated wheel loading remains limited. This study investigated the influence of geogrid placement on pavement response using full-scale Accelerated Pavement Testing. Three pavement sections were constructed over a weak subgrade with a California Bearing Ratio of approximately 5%: an unreinforced control section (A1), a section reinforced at the subgrade-subbase interface (A2), and a section reinforced at the top of the granular subbase layer beneath the asphalt binder course (A3). All sections had identical layer configurations and were subjected to 3,000,000 load repetitions under field temperature conditions. Performance was evaluated using rut depth, transverse surface deformation profiles, vertical stress near the top of the subgrade, and tensile strain at the bottom of the asphalt layer. Reinforcement improved all measured responses, with location strongly affecting performance. Section A3 showed the best behavior, reducing rut depth from 21.5 mm in A1 to 12.1 mm, while giving the lowest final vertical stress, 46.73 kPa, and tensile strain, 154.7 με. These results indicate that placing geogrid at the top of the subbase layer was most effective under the tested full-scale loading conditions.

1. Introduction

The structural and functional performance of flexible pavements is continuously affected by repeated traffic loading and environmental actions. Rutting is considered one of the most critical distress modes in flexible pavements, particularly in regions with high pavement temperatures and heavy axle loads, where permanent deformation accumulates in both asphalt and unbound layers [1,2]. Therefore, improving rutting resistance and controlling stress–strain distribution within pavement structures remains essential for extending service life and reducing maintenance costs. Geosynthetic reinforcement, particularly biaxial geogrids, has been increasingly used to improve the structural behavior of flexible pavements constructed over weak subgrades. The main reinforcement mechanisms include lateral confinement of aggregate particles, improved aggregate interlock, wider load distribution, and the development of tensioned membrane effects under deformation [3-5].

Large-scale laboratory investigations and review studies have shown that geogrid performance is influenced by tensile stiffness, aperture geometry, placement location, unbound aggregate layer thickness, and subgrade strength [6,7]. Although laboratory evidence indicates measurable improvements in rutting resistance with geogrid stabilization, it is difficult to translate such findings to field-scale behavior due to scale effects and boundary-condition limitations [8]. Full-scale Accelerated Pavement Testing (APT) provides an effective approach for bridging this gap by

*Corresponding author: bce.22.23@grad.uotechnology.edu.iq
[a]orcid.org/0009-0002-5442-9411; [b]orcid.org/0000-0001-7836-1525; [c]orcid.org/0000-0001-8028-731X
DOI: http://dx.doi.org/10.17515/resm2026-1692st0519rs

applying controlled moving wheel loads within a reduced time period while maintaining realistic structural configurations [9,10]. Recent full-scale APT studies have reported reductions in rutting and subgrade stress in geogrid-reinforced pavement sections compared with unreinforced control sections [11,12].

The interpretation of accelerated testing results demands robust instrumentation to measure rut depth, tensile strain at critical asphalt interfaces, and vertical stress transmitted to underlying layers [13]. Previous studies have emphasized the importance of advanced monitoring techniques and well-designed data acquisition systems for accurate structural evaluation under repeated loading [14]. Moreover, it has been shown that combining experimental measurements with mechanistic understanding and numerical modeling improves the interpretation of reinforcement mechanisms and long-term performance prediction [15, 16]. Although the benefits of geogrid reinforcement are established, full-scale evidence that isolates reinforcement location while simultaneously tracking surface deformation, subgrade stress, and asphalt tensile strain under a common loading and temperature history remains limited. The specific novelty of this study is the direct comparison of two practically relevant geogrid locations within adjacent full-scale sections on the same circular APT track. Because all sections were trafficked during the same device revolutions, the study links reinforcement position to a coherent set of external and internal structural responses rather than to rut depth alone.

Accordingly, this study investigates the effect of geogrid reinforcement location on rut-depth progression, transverse surface deformation, vertical stress near the top of the subgrade, and tensile strain at the bottom of the asphalt binder course. The results provide full-scale comparative evidence on how reinforcement position modifies the load-transfer pathway under repeated wheel loading and field temperature exposure.

2. Full-Scale Accelerated Pavement Testing Program

2.1 Description of the Accelerated Pavement Testing Facility

The experimental program was conducted using a purpose-built circular Accelerated Pavement Testing (APT) device designed and fabricated for full-scale pavement-performance evaluation. The loading system consists of a circular track with a circumference of 16.2 m, allowing continuous wheel movement along a fixed trafficking path.

Fig. 1. Photograph of the locally fabricated circular Accelerated Pavement Testing (APT) device

A 10-hp motor drives the loading carriage through a mechanical gearbox, providing uniform torque transmission and controlled rotational speed. A pneumatic dual-wheel assembly applies a constant 25 kN load at a tire inflation pressure of 60 psi (approximately 414 kPa). The wheels travel at 20 km/h, and the constant-amplitude loading system maintains the same applied load during each operating phase. Figure 1 shows the circular APT system. Its continuous circular path avoids the acceleration and deceleration boundary effects associated with short linear loading devices.

2.2 Construction of Full-Scale Pavement Sections

Three full-scale pavement sections were constructed consecutively along the same circular loading track at the Accelerated Load Test Pavement facility in Karbala City, Iraq. All sections had the same structural configuration: compacted natural subgrade, a 300 mm granular subbase, a 50 mm asphalt binder course, and a 40 mm asphalt wearing course. Figure 2 presents both the cross-sectional configurations and the common circular-track plan view. Section A1 was constructed as an unreinforced control section. In Section A2, a biaxial geogrid was placed at the subgrade–subbase interface, directly above the compacted natural subgrade and beneath the granular subbase layer. In Section A3, the same biaxial geogrid was placed at the top of the granular subbase layer, directly beneath the asphalt binder course. This configuration was adopted to evaluate the influence of geogrid reinforcement location on pavement response under repeated wheel loading.

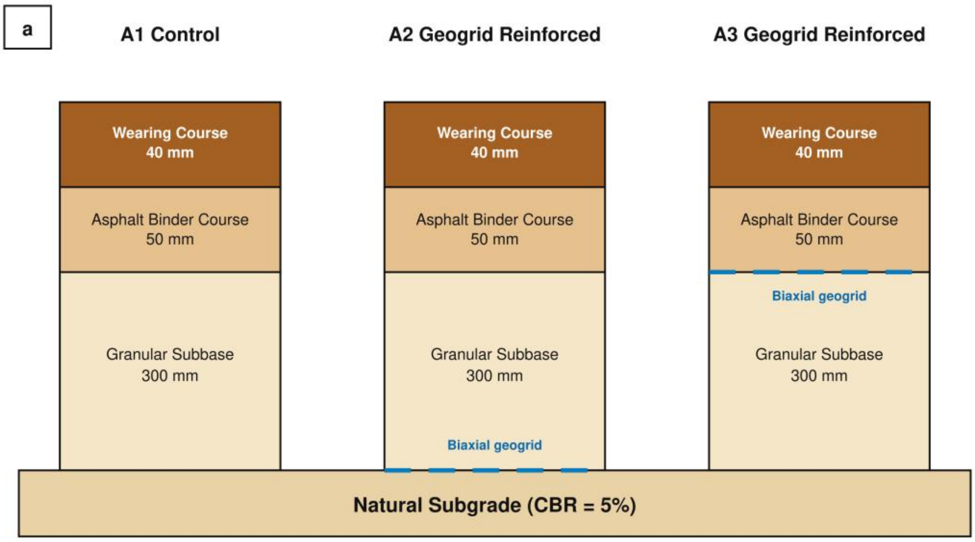

(a)

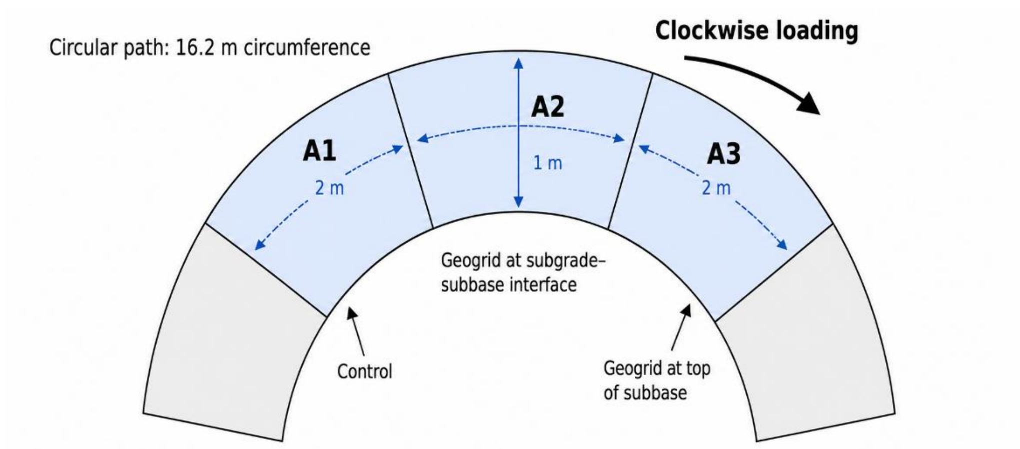

(b)

Fig. 2. Experimental layout: (a) cross-sectional configurations of Sections A1–A3 and geogrid locations; (b) plan view showing the consecutive sections on the common circular loading path and the clockwise loading direction

A rigid slab was not included because its high flexural stiffness would change the investigated system from a conventional flexible pavement to a composite pavement governed mainly by slab action and slab–foundation interaction. Its exclusion was necessary to isolate the effect of geogrid location within the granular support system. Geogrid behavior in composite pavement systems may be investigated in future studies. The granular subbase was placed in two successive lifts of approximately 150 mm. Moisture was adjusted near the optimum moisture content, and each lift was compacted with a vibratory steel-drum roller. In-situ density was checked using the sand-cone method (ASTM D1556), and a minimum of 95% of the maximum dry density was required. Layer elevation and thickness were checked before placement of the overlying course so that all sections provided comparable support conditions.

2.3 Subgrade and Material Properties

The natural subgrade soil used in the construction of the pavement sections was classified as low-plasticity clay according to the Unified Soil Classification System (USCS) and as A-6 according to the AASHTO classification system. The main engineering properties of the natural subgrade soil are summarized in Table 1. The California Bearing Ratio (CBR) of the subgrade was approximately 5%, indicating the weak support condition adopted in this study. This clay was deliberately selected because it represents a locally encountered weak cohesive subgrade. The principal experimental design criterion was to provide a uniformly weak foundation with a CBR of approximately 5%, allowing the influence of geogrid location to be evaluated under a demanding support condition. The same subgrade condition was used for all pavement sections to ensure that the observed differences in performance were mainly related to the geogrid reinforcement configuration rather than variations in foundation support.

Table 1. Physical and mechanical properties of pavement construction materials

Material	Property	Value	Unit	Standard / Specification
Coarse Aggregate	Bulk Specific Gravity	2.684	—	ASTM C127
	Apparent Specific Gravity	2.763	—	ASTM C127
	Water Absorption	0.512	%	ASTM C127
	Los Angeles Abrasion	19.2	%	ASTM C131 (≤ 30)
	Soundness Loss (Na_2SO_4)	4.1	%	ASTM C88 (≤ 10)
Fine Aggregate	Bulk Specific Gravity	2.731	—	ASTM C128
	Apparent Specific Gravity	2.821	—	ASTM C128
	Water Absorption	0.773	%	ASTM C128
Mineral Filler (Limestone Dust)	Bulk Specific Gravity	2.85	—	—
	Passing No. 200 Sieve	94	%	—
	Specific Surface Area	595	m^2/kg	—
Asphalt Cement (40–50 Penetration Grade)	Penetration (25°C, 100g, 5s)	42–43	0.1 mm	ASTM D5 (40–50)
	Ductility (25°C)	138–147	cm	ASTM D113 (>100)
	Softening Point (R&B)	49–51	°C	ASTM D36
	Flash Point (COC)	283–290	°C	ASTM D92 (≥232)
Subgrade Soil	Specific Gravity at 25°C	1.039–1.041	—	ASTM D70
	Liquid Limit (LL)	42	%	ASTM D4318
	Plastic Limit (PL)	15	%	ASTM D4318
	Plasticity Index (PI)	27	%	ASTM D4318
	Optimum Moisture Content (OMC)	11	%	ASTM D698
	Maximum Dry Density (MDD)	1.78	g/cm^3	ASTM D698
California Bearing Ratio	(CBR)	5	%	ASTM D1883

The granular subbase material consisted of well-graded crushed aggregate complying with the relevant specification requirements. The asphalt binder used in the conventional sections was a 40-50 penetration grade asphalt cement. The asphalt mixture for Sections A1, A2, and A3 was designed according to the Marshall method. The optimum asphalt content of the adopted mixture was 5%. The adopted job mix formula yielded a Marshall stability of 9.15 kN, bulk density of 2.29 g/cm^3, air void content of 3.79%, flow value of 3.34 mm, VMA of 16.8%, and VFA of 78%. The physical and mechanical properties of the construction materials are summarized in Table 1.

2.4 Geogrid Properties and Installation

A biaxial polypropylene geogrid was used as reinforcement in Sections A2 and A3. Polypropylene was selected because it is lightweight and resistant to moisture, biological degradation, and chemicals commonly present in soils. It also permits the production of a biaxial geogrid that provides balanced reinforcement in both principal directions. The selected product had 40 mm apertures, a tensile strength of 30 kN/m in both directions, and a junction efficiency of 93%, which promotes aggregate interlock and lateral confinement. The same polypropylene geogrid was used in A2 and A3 because the study was designed to isolate the effect of reinforcement location rather than polymer type.

Fig. 3. Locations of geogrid reinforcement within the pavement structure (subgrade–subbase interface and top of subbase layer)

Table 2. Physical and mechanical properties of the biaxial geogrid

Item	Test Method	Unit	PPX3030	
			MD	TD
Polymer	-	-	PP	PP
Type			Knitted coated with a durable polymer	
Minimum Carbon Black	ASTM D 4218	%	2	
Aperture Size		mm	40	40
Tensile Strength	ASTM D 6637	kN/m	30	30
Tensile Strength @ 2% Strain	ASTM D 6637	kN/m	10.5	10.5
Tensile Strength @ 5% Strain	ASTM D 6637	kN/m	21	21
Elongation	ASTM D 6637	%	13	13
Junction Efficiency	GRI GG2	%	93	93
Flexural Rigidity	ASTM D 7748	mg-cm	2,000,000	
Aperture Stability	ASTM D 7864	m-N/deg	0.75	
Roll Width	-	m	3.95	
Roll Length	-	m	50	

In Section A2, the geogrid was installed at the subgrade–subbase interface, directly above the compacted natural subgrade. In Section A3, the geogrid was placed at the top of the granular subbase layer, immediately beneath the asphalt binder course. The physical and mechanical properties of the geogrid, including tensile strength, aperture size, and elongation characteristics, are presented in Table 2. During installation, the geogrid was tensioned and secured to eliminate wrinkles and ensure full surface contact with the subgrade. Subbase material was placed carefully to prevent displacement or damage to the reinforcement layer.

2.5 Instrumentation and Data Acquisition System (DAQ)

An integrated instrumentation system was installed after the construction of the pavement sections to monitor rutting, tensile strain, subgrade stress and temperature under accelerated loading. All sensors were attached to a centralized data acquisition system to allow synchronized recording of the dynamic responses.

2.5.1 Subgrade Load Cells

The vertical stress acting on the subgrade was measured with LCF Series soil load cell transducers (Omega Engineering). One load cell was installed 5 cm beneath the subbase interface along the wheel path in each section. Each load cell had a diameter of 100 mm and a rated load capacity of 500 kN. Each cell was enclosed in a fine sand cushion prior to placing the subbase, to ensure uniform stress distribution. Stress pulses in the load cells were transient and were produced by wheel passage, which allowed comparison of stress decay between reinforced and control sections.

Fig. 4. Installation of the subgrade load cell used for vertical stress measurement

2.5.2 Asphalt Strain Gauges

The ASG 3000-H strain gauges (TML) for measuring horizontal tensile strains in the asphalt layers are designed for high temperature pavement applications. The resistance of each gauge was 350 Ω, with an effective length of 120 mm. One strain gauge was installed in each section at the bottom of the asphalt binder course, directly above the granular subbase layer. This arrangement enabled tensile strain to be measured at the critical fatigue-related location under repeated wheel loading.

Fig. 5. Installation of asphalt strain gauges for tensile strain monitoring

2.5.3 Linear Variable Differential Transformers (LVDTs) for Rut Depth Measurement

Surface rutting was measured using DCTH Series LVDTs (RDP Electronics). Two LVDTs were installed per section and mounted on a rigid reference beam aligned with the wheel path. Each sensor had a measurement range of 0–100 mm and an accuracy of ±0.01 mm. Continuous deformation data were recorded to track rut progression throughout the loading program.

Fig. 6. Installation of Linear Variable Differential Transformers (LVDTs) for rut depth measurement

2.5.4 Temperature Monitoring and Data Acquisition

Thermocouples embedded within the asphalt layer continuously recorded pavement temperature to account for temperature-dependent material behavior. All sensors were connected to a TDS-530 Data Acquisition System operating at sampling rates between 100 Hz and 1 kHz. The system included signal conditioning modules to ensure accurate, noise-free measurement of dynamic pavement responses.

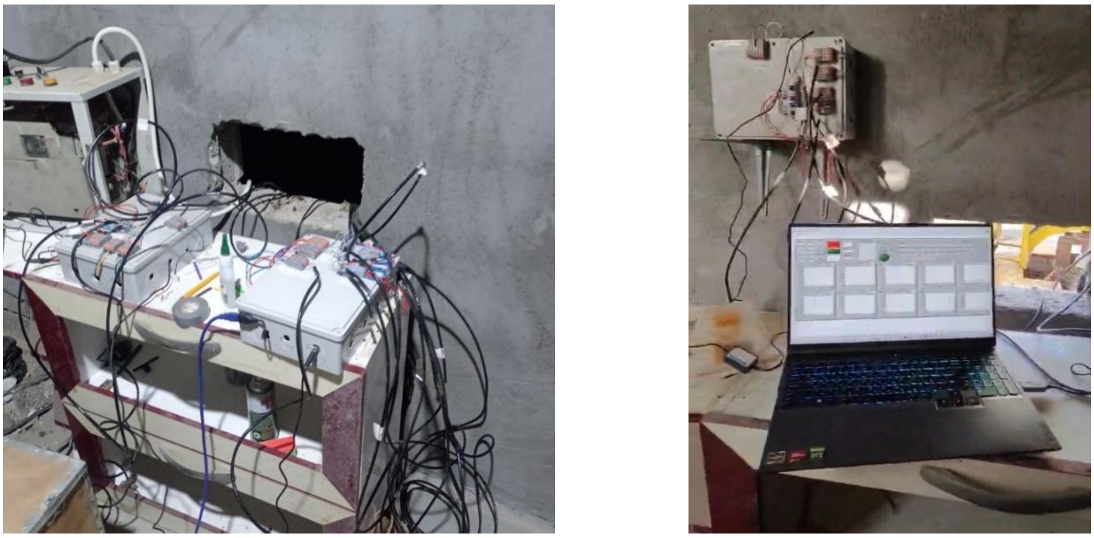

Fig. 7. (DAQ) showing connections between load cells, strain gauges, LVDTs, and thermocouples

2.5.5 Measurement Reliability and Quality Control

Before the main loading program, the loading assembly, wheel path, sensors, and data-acquisition channels were checked through trial operation. Each sensor channel was identified according to its test section and measured response, checked for electrical continuity, and zeroed under the no-load condition. The LVDT outputs were checked for smooth response over their working range and for stable baseline readings. Their contact tips and reference beams were also inspected to prevent seating movement during testing. The load-cell and asphalt-strain-gauge channels were examined during repeated trial wheel passages to confirm continuous and repeatable response pulses. Thermocouple readings were checked for consistency with the prevailing pavement and ambient temperature conditions.

Quality-control procedures continued throughout the loading program through periodic checks of tire pressure, operating speed, wheel tracking, cable protection, sensor baselines, signal noise, missing readings, and abnormal drift. The LVDTs had a manufacturer-specified accuracy of ±0.01 mm. The stress and strain measurements were evaluated according to the stated transducer specifications, stable baseline response, and repeatability of the recorded wheel-load pulses. A formal combined uncertainty analysis was not performed for the embedded stress and strain sensors; therefore, the reported differences are interpreted as controlled comparative measurements rather than absolute metrological estimates. The use of the same loading device, data-acquisition system, sampling procedure, and environmental exposure for Sections A1–A3 reduced systematic differences among the tested sections [10,13,14,17].

2.6 Accelerated Loading Program

Upon construction and instrumentation, the pavement sections were subjected to repeated loading using a circular APT device under constant amplitude loading conditions. The magnitude of the applied dual-wheel load was 25 kN. The tire inflation pressure was controlled to be 60 psi (approximately 414 kPa), and the wheel speed was controlled to be 20 km/h. The circular trafficking path had a circumference of 16.2 m, and a total of 3,000,000 load repetitions were applied during the test program. Sections A1, A2, and A3 were tested concurrently rather than sequentially. The three sections formed consecutive segments of the same circular trafficking path; therefore, during each complete revolution of the APT device, the same dual-wheel assembly passed over all three sections. Consequently, all sections received the same number of load repetitions and were subjected to identical wheel-load, tire-pressure, speed, and operating conditions.

The test was carried out under actual field conditions from July to December 2025. Pavement temperature was continuously monitored throughout the loading program. The average monthly pavement temperature decreased from high summer values to lower winter values, ranging from 53.36 °C during August to 21.17 °C during December. Therefore, the measured pavement responses should be interpreted as the combined effect of repeated wheel loading, pavement temperature variation, and geogrid reinforcement configuration. Because all sections were trafficked during the same device revolutions on the same circular track, they were exposed to the same seasonal temperature history. Therefore, temperature affected the overall development of the measured responses but did not create a difference in environmental exposure among Sections A1, A2, and A3. The observed differences are mainly attributed to the geogrid configuration and placement location.

3. Results and Discussion

3.1 Pavement Temperature During the Testing Period

The accelerated pavement testing program was conducted under actual field conditions from July to December 2025. During this period, pavement temperature was monitored continuously to support the interpretation of rutting, stress, and strain responses. The average monthly pavement temperature was 53.06 °C in July, 53.36 °C in August, 45.92 °C in September, 38.68 °C in October, 28.74 °C in November, and 21.17 °C in December. These values indicate that the pavement sections were subjected to a wide range of temperatures, decreasing gradually from high summer temperatures to cooler winter conditions.

At high pavement temperature, the asphalt layer had lower stiffness and greater susceptibility to permanent shear deformation. Cooling during later loading stages increased asphalt stiffness and probably reduced the incremental rate of rutting; however, deformation, stress redistribution, and tensile strain continued to accumulate under repeated wheel passages. Temperature is therefore treated as a common time-varying exposure, not as an uncontrolled difference among the three sections.

Because A1–A3 were trafficked concurrently on the same circular path, their direct comparison remains valid at each common load count. Subsequent sections therefore refer to the shared temperature history summarized here rather than repeating the full temperature discussion.

Table 3. Average monthly pavement temperature during the accelerated loading period

Month	Average pavement temperature (°C)
July	53.06
August	53.36
September	45.92
October	38.68
November	28.74
December	21.17

3.2 Transverse Surface Deformation Profiles

The deformation profiles in all sections gradually evolved into a clear W-shaped pattern with two depressions occurring under the wheel paths and an upward heave between and outside the loading zones. This pattern is caused by the combined effects of repeated densification and lateral movement of material within the asphalt and unbound layers under wheel loading.

The distance between successive deformation profiles grew with the number of load repetitions, indicating permanent deformation accumulated progressively in all sections. The magnitude and shape of the deformation profiles, however, were different for each pavement configuration. The unreinforced control section generally exhibited the largest deformation, while the reinforced sections exhibited smaller depressions and less heave. The results indicated that the geogrid reinforcement and particularly its position in the pavement structure, had a significant effect on the transverse deformation response under repeated loading.

A rut depth of 12.5 mm was adopted as a serviceability threshold based on a commonly used FHWA pavement-performance benchmark. This level represents a maximum allowable rut depth used to identify potential serviceability and safety concerns, including water accumulation and hydroplaning. In the present APT program, it was used as a consistent comparative benchmark for determining the number of load repetitions at which each section reached the same rutting level, rather than as an indication of sudden structural failure [18].

3.3 Performance of the Control Section (A1)

The surface deformation profiles of the control section without geogrid reinforcement are shown in Fig. 9. This section exhibited the most severe rutting of the three configurations tested. The profile at the beginning of the test was almost flat, indicating that all sections started from a similar undeformed state. With increasing load repetitions, the rut depth increased progressively and the profile became steeper beneath the wheel paths.

During the last loading stage, the maximum depression in the control section was approximately 21.5 mm, which exceeded the adopted serviceability-failure threshold shown in the figure. The control section exceeded this threshold relatively early, between approximately 1.0 and 1.5 million load repetitions. This exceedance indicates a loss of acceptable pavement serviceability under repeated wheel loading rather than sudden structural collapse.

The significant lateral flow of pavement materials is also evident in the pronounced upward heave between the two wheel paths and along the outer edges. Under traffic simulation, the aggregate particles were able to laterally move and rearrange because the granular layer and top of the subgrade in the unreinforced section had lower resistance to repeated shear stresses. Thus, the rutting mechanism in A1 appears to be controlled by the combined effect of densification within the pavement layers and shear deformation in the weak supporting layers.

3.4 Performance of the Geogrid-Reinforced Section at the Subgrade Interface (A2)

Deformation profiles for section A2, where the geogrid was placed at the subgrade–subbase interface, are shown in Fig. 10. This configuration exhibited a clear reduction in rut depth for the entire loading program compared to the control section. Even though the rutting still increased with the number of cycles, the shape of the deformation was always shallower than A1. The maximum rut depth in A2 was 16.5 mm at the end of the test and lower than the control section (21.5 mm). This corresponds to a rut reduction of about 23.3% in comparison to A1 at the last loading stage. Moreover, the adopted serviceability-failure threshold of 12.5 mm was exceeded later than in the control section, indicating that the geogrid reinforcement improved rutting resistance and extended the serviceable life of the pavement section under repeated loading.

The central and outer shoulder heave was also reduced in A2 compared to A1. This means that the geogrid limited the lateral spreading of the granular layer and provided better confinement at the bottom of the unbound system. The reinforcement when placed directly on the top of the subgrade helped to distribute the applied wheel load over a greater area and reduce the stress concentration on the weak subgrade. So, subgrade intrusion and accumulation of permanent deformation were reduced, compared with the unreinforced section.

Overall, the rutting performance of section A2 was improved considerably compared to the control section. However, its final rut depth was higher than the one recorded in section A3. This implies that geogrid placement at the subgrade–subbase interface was beneficial but less effective than placement at the top of the granular subbase layer, under the present testing conditions.

3.5 Performance of the Geogrid-Reinforced Section at the Top of the Subbase (A3)

Deformation profiles for section A3 with the geogrid placed at the top of the granular subbase layer are shown in Fig. 11. This section also outperformed the control section, reinforcing the beneficial effect of geogrid reinforcement on pavement response under repeated loading. Results show that A3 provided the best rutting performance of the three investigated sections. The maximum final rut depth in A3 was 12.1 mm, which is lower than both the control section and section A2. This corresponds to a a rut reduction of approximately 43.7% compared to Section A1 at the end of the loading program. The results of this study suggest that the use of the geogrid in the top of the granular subbase layer was a more effective configuration for limiting the permanent surface deformation under the current loading conditions.

Table 4. Integrated comparison of final structural responses and reductions relative to A1

Section	Configuration	Rut depth (mm)	Rut reduction (%)	Subgrade stress (kPa)	Stress reduction (%)	Tensile strain (με)	Strain reduction (%)
A1	Control, unreinforced	21.5	—	56.68	—	194.2	—
A2	Geogrid at subgrade–subbase interface	16.5	23.3	48.82	13.9	169.5	12.7
A3	Geogrid at top of granular subbase	12.1	43.7	46.73	17.6	154.7	20.3

A3 also showed a reduction in the magnitude of the central and edge heave compared to A1, which means that the reinforcement at the upper subbase level helped to limit material shoving and lateral displacement. Moreover, the deformation profiles suggest that this configuration was more stable in the transverse surface shape over the loading program than the other sections. This behavior indicates that the geogrid in A3 improved the confinement of the upper granular zone and was more effective in controlling the rut development.

Table 4 integrates the final rut depth, subgrade stress, and asphalt tensile strain and their percentage reductions relative to A1. The consistent ranking—A3, A2, then A1—shows that the surface and internal responses were linked rather than independent outcomes. Because Section A3 was subjected to the same loading sequence and pavement temperature history as Sections A1 and A2, its lower final rut depth indicates that the improvement was mainly associated with the reinforcement location rather than differences in environmental exposure.

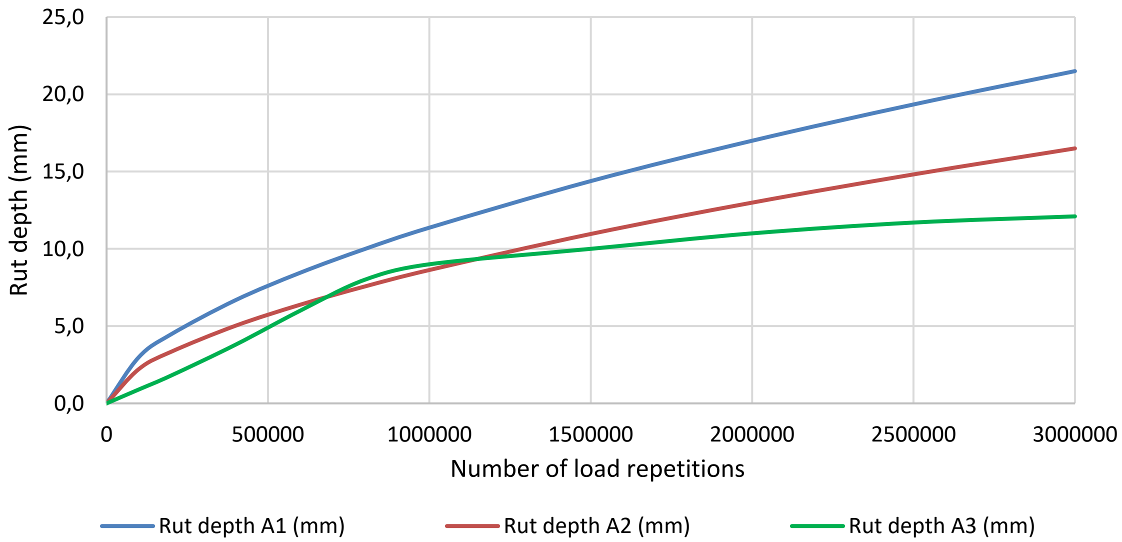

Fig. 8. Rut depth progression versus number of load repetitions for the tested pavement sections.

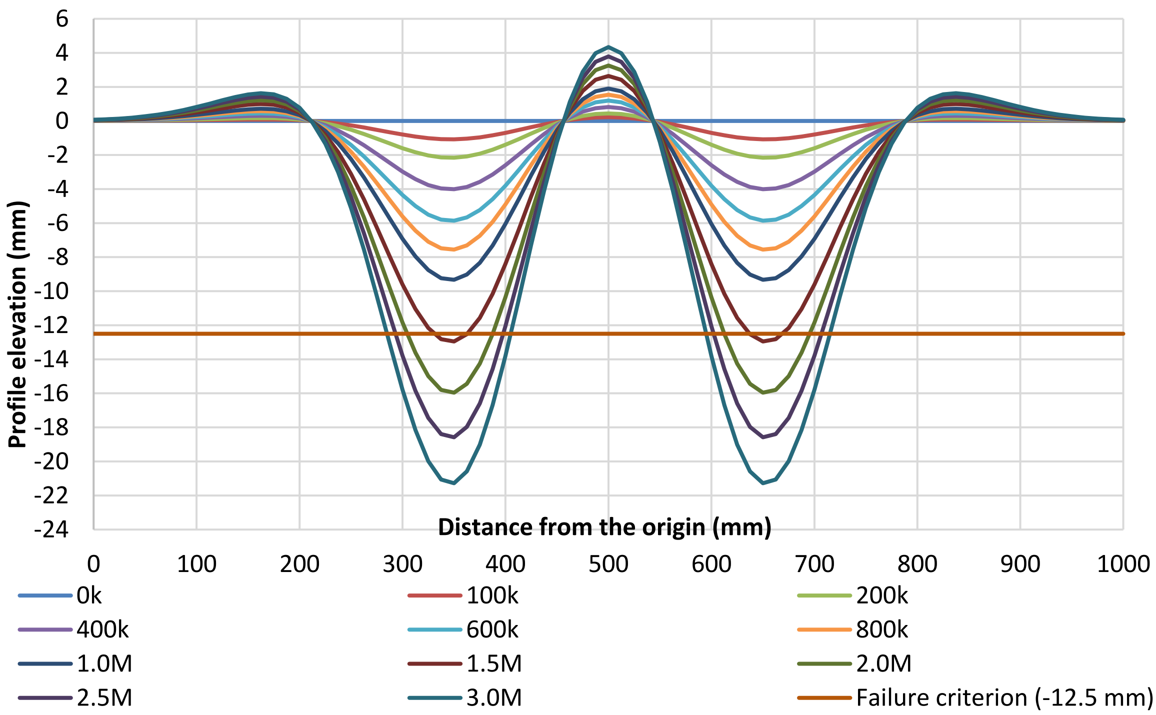

Fig. 9. Transverse surface-deformation profiles for A1 at selected loading stages. The 0k curve is the initial pavement surface before loading

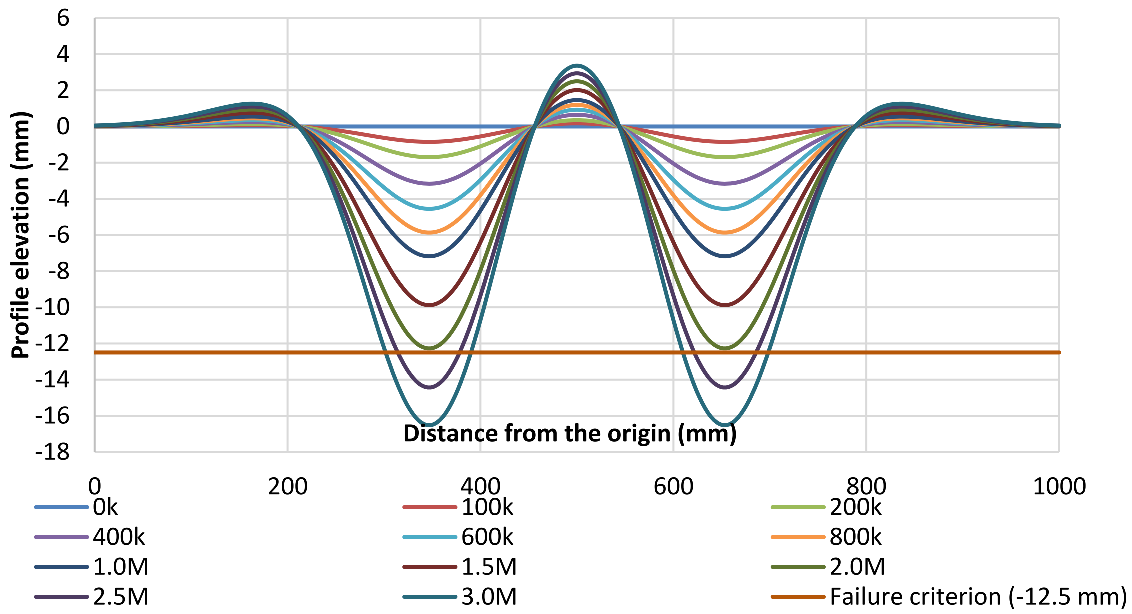

Fig. 10. Transverse surface-deformation profiles for A2 at selected loading stages. The 0k curve is the initial pavement surface before loading

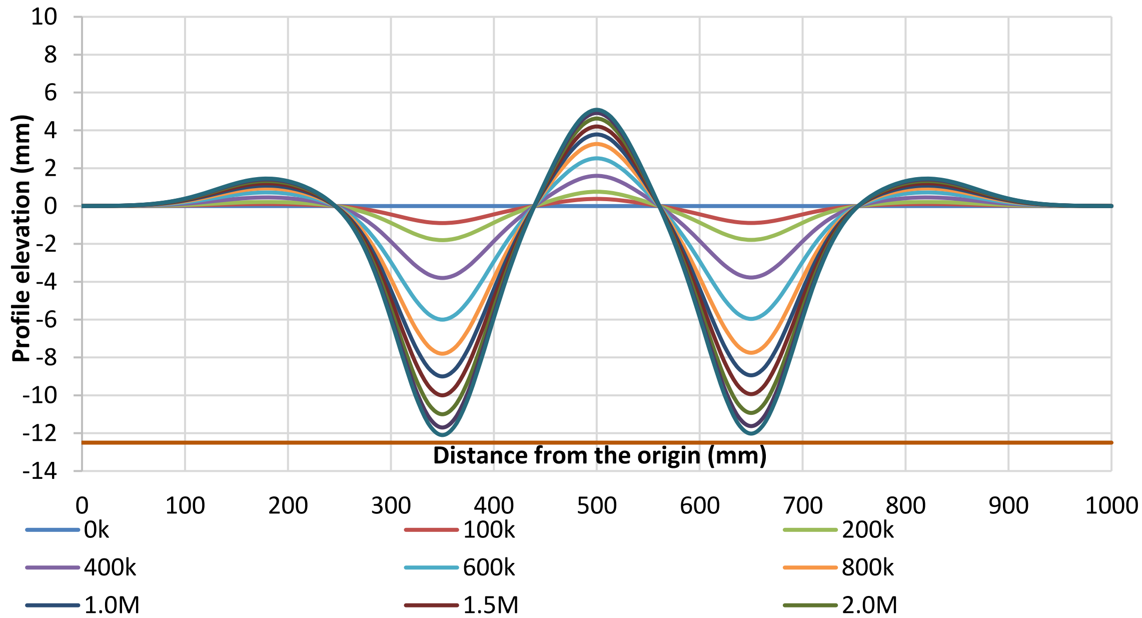

Fig. 11. Transverse surface-deformation profiles for A3 at selected loading stages. The 0k curve is the initial pavement surface before loading

3.6 Mechanistic Interpretation

The improved rutting resistance of the reinforced pavement sections agrees well with earlier experimental and numerical studies on geogrid-reinforced pavement systems [19,20]. The addition of geogrid reinforcement improves the aggregate interlock and confinement in the granular layers, leading to better load distribution and reduced stress concentration on the weak subgrade [21-23]. Previous laboratory dynamic-load studies on flexible pavement sections reinforced with geogrid also reported that the presence of geogrid reduces transmitted vertical stresses and surface displacement, especially when the reinforcement is placed within the granular layer or at the base-subgrade interface [24,25].

Both the reinforced sections in the present study showed lower rut depth than the unreinforced control section, confirming the positive role of geogrid reinforcement under repeated loading.

However, results also show that the location of the reinforcement clearly affected the extent of improvement obtained. In Section A2, placing the geogrid at the subgrade–subbase interface limited the stress concentration at the top of the subgrade and provided better confinement near the weak foundation layer, resulting in less rut development than in A1. Of the three tested sections, the section with geogrid placed on top of the granular subbase layer (Section A3) showed best performance in terms of rutting. This behavior indicates that the reinforcement at the upper subbase level was more effective in controlling the deformation in the upper unbound zone and in limiting the accumulation of permanent surface deformation under the current loading conditions. The better response of A3 might be due to the improved confinement of the upper granular layer, which reduced lateral displacement and maintained a more stable transverse surface profile under repeated loading.

The results generally indicated that the use of geogrid reinforcement improved the structural response of the pavement; however, the effectiveness of the reinforcement was dependent on the reinforcement location in the pavement system. The geogrid placed at the top of the granular subbase layer gave the best performance in terms of rutting resistance for the conditions considered in this study, while placement at the subgrade–subbase interface still resulted in a significant improvement over the unreinforced section. The three measured responses can be interpreted through a common load-transfer mechanism. Under repeated wheel loading, lateral spreading of the granular particles reduces aggregate confinement and concentrates the applied load over a smaller area. This process contributes to permanent surface rutting, increases the vertical stress transmitted to the subgrade, and produces less uniform support beneath the asphalt layer, thereby increasing asphalt bending and bottom tensile strain. The geogrid limits lateral aggregate movement through aggregate–aperture interlock and tensile restraint, allowing the wheel load to be distributed over a wider area.

In Section A2, the geogrid was located at the subgrade–subbase interface, beneath the full 300 mm thickness of the granular subbase. This position restrained aggregate spreading and reduced intrusion near the weak clay subgrade. However, part of the wheel-induced shear deformation could develop within the upper granular layer before the load reached and mobilized the reinforcement. In Section A3, the geogrid was placed immediately beneath the asphalt binder course and closer to the zone of high shear stress and differential movement. Therefore, aggregate interlock was mobilized earlier in the load-transfer path, restricting lateral displacement of the upper subbase and improving the support provided directly beneath the asphalt layer. This difference in load-transfer behavior explains the consistent relationship among the measured responses. Relative to the control section A1, Section A2 reduced the final rut depth, subgrade stress, and asphalt tensile strain by 23.3%, 13.9%, and 12.7%, respectively, whereas Section A3 reduced them by 43.7%, 17.6%, and 20.3%, respectively. Thus, the lower rut depth, reduced subgrade stress, and decreased asphalt tensile strain in A3 are structurally connected consequences of earlier reinforcement engagement and wider load distribution within the pavement structure.

3.7 Vertical Stress at the Top of the Subgrade

Fig. 12 shows the variation of vertical stress transmitted to the top of subgrade for the three pavement sections. The stresses were measured by means of load cells installed directly below the wheel path at a depth of 5 cm below the subbase interface. The measured stresses in all sections were relatively close in the early stages of loading, indicating that the pavement structures responded in a similar manner at the beginning of the applied wheel load. With the increase in the number of repetitions of load, however, differences appeared between the reinforced and unreinforced sections. The short initial drop and fluctuation in vertical stress are attributed to bedding-in of the pavement system and pressure-cell seating. Early wheel passages rearranged aggregate contacts, completed local densification, and improved contact around the fine-sand cushions enclosing the cells, temporarily redistributing the local stress field. Because the signals remained continuous and subsequently stabilized into consistent section-specific trends, this early behavior was interpreted as an initial seating/stabilization effect rather than sensor failure.

The vertical stress in the control section (A1) gradually increased with the increase of load repetitions. The stress level increased from approximately 49 kPa at the start of the test to almost 56.68 kPa after three million load cycles. The trend indicates that the unreinforced pavement structure progressively densified and its ability to distribute load diminished as permanent deformation accumulated. Meanwhile, the stress levels were relatively lower in the geogrid-reinforced sections than the control section during almost the whole loading program, which indicated the positive effect of geogrid reinforcement on improving the load distribution and reducing the stress concentration on the weak subgrade. At the end of the test, the vertical stress recorded in section A2 was 48.82 kPa and 46.73 kPa in section A3, showing that both reinforcement configurations reduced the stress transmission compared to the unreinforced section. Relative to the control section, these values correspond to final vertical stress reductions of approximately 13.9% and 17.6% for A2 and A3, respectively. This trend is consistent with previous model tests in which geogrid reinforcement reduced transmitted stress by about 23.5-42.8% when placed in the middle of the base course, and by about 20.4-39.4% when placed at the interface between the base and subgrade [25].

A recent scaled-model study of geotextile-reinforced flexible pavements over weak clay subgrade similarly reported lower transmitted subgrade stresses in the reinforced sections and demonstrated that reinforcement location influenced the magnitude of the improvement [26]. It is clear that the stress transmitted to the subgrade in Section A2, where the geogrid was placed at the subgrade–subbase interface, was significantly reduced. The measured stress decreased in the early loading stages and then remained relatively stable in later stages of the test. This behavior indicates that the geogrid provided better confinement at the weak foundation layer and helped to better distribute the load within the pavement structure. Among the three sections, A3 produced the lowest final stress. Locating the geogrid at the top of the subbase improved load sharing in the upper pavement structure and reduced the magnitude of stress transmitted to the weak supporting layer. Both reinforcement configurations improved the response relative to A1, but A3 provided the most favorable stress reduction, followed by A2.

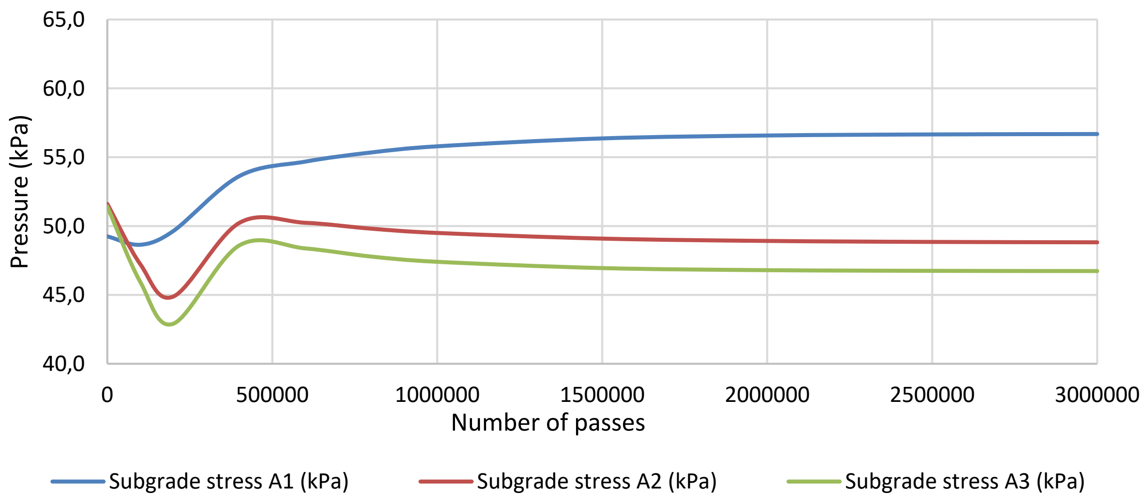

Fig. 12. Vertical stress at the top of the subgrade versus number of load repetitions

3.8 Tensile Strain at the Bottom of the Asphalt Binder Course

The tensile strain at the bottom of the asphalt binder course is an important parameter for evaluating the fatigue performance of flexible pavements. In the present study, asphalt strain gauges were embedded in the pavement sections to measure the tensile strain responses under repeated wheel loading. A strain gauge was installed at the bottom of the asphalt binder course to record the tensile strain caused by each wheel pass. The tensile strain variation with the increase of load repetitions for the three pavement sections is presented in Fig. 13. In the early loading stage, the strain measurements fluctuated significantly due to the initial adjustment and densification of the asphalt and granular layers under repeated loading. Following this initial phase, the strain responses gradually levelled off and a clearer trend emerged.

The control section (A1) generally had higher tensile strain levels as compared to the reinforced sections, indicating that the absence of reinforcement resulted in higher strain concentrations at the bottom of the asphalt layer. Generally, as tensile strains increase, the risk of fatigue cracking increases and the pavement service life decreases. At the end of the test, the tensile strain in the control section was 194.2 με. The reinforced sections showed an improved strain response compared with the control section. Section A2, where geogrid was placed at the subgrade–subbase interface, showed a considerable reduction in tensile strain during the loading program. The last tensile strain measured in A2 was 169.5 με, representing a reduction of about 12.7% as compared to the control section. This behavior indicates that the geogrid improved load distribution through the pavement structure and reduced tensile strain development in the asphalt layer.

Section A3, in which the geogrid was placed at the top of the granular subbase layer, was the section with the minimum tensile strain of the three sections tested. The final tensile strain of A3 was 154.7 με, representing a reduction of about 20.3% compared with A1. The results show that, under the present testing conditions, the geogrid at the top of the granular subbase layer gave the most favorable structural response by reducing the tensile strain at the bottom of the asphalt layer. This indicates that the reinforcement in A3 was more effective in reducing the bending demand and improving the support conditions beneath the asphalt layer under repeated loading. Overall, geogrid reinforcement reduced tensile strain at the bottom of the asphalt layer and may therefore delay fatigue-crack initiation. A3 showed the best response, followed by A2, while A1 was the least favorable. The ranking confirms that reinforcement location affected the internal strain response of the pavement system.

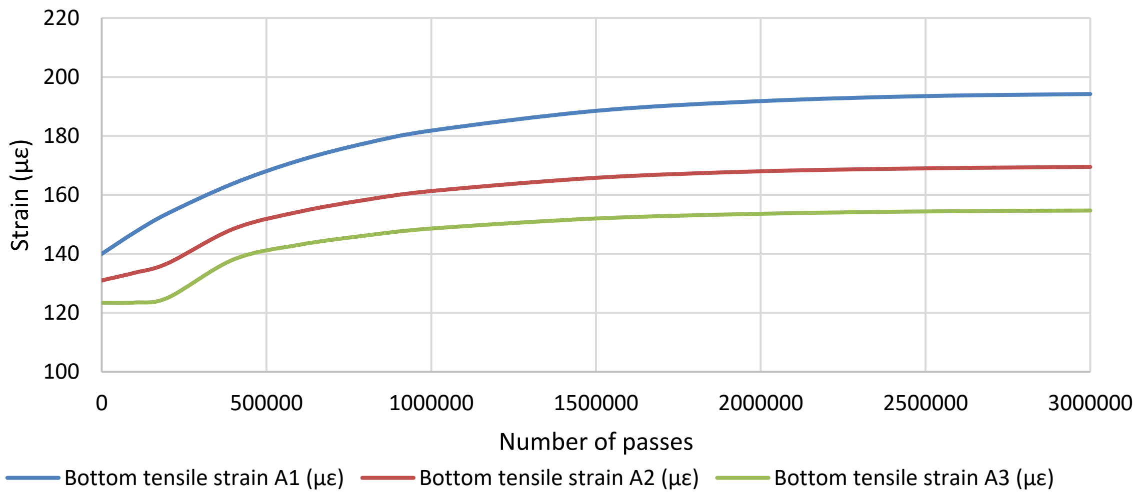

Fig. 13. Tensile strain at the bottom of the asphalt binder course versus number of load repetitions

3.9 Study Limitations

The results of this study should be interpreted within the limitations of the experimental program. The accelerated pavement testing was conducted under actual field conditions from July to December 2025, during which pavement temperature decreased substantially. Therefore, the measured responses represent the combined effects of repeated loading, seasonal pavement temperature variation, and reinforcement configuration. This interpretation agrees with finite element analysis of flexible pavement under combined wheel and thermal loads, where increasing wheel pressure increased vertical displacement and the thermal field modified the pavement response [27]. In addition, each pavement configuration was represented by one full-scale section. Thus, the results are best considered as controlled full-scale comparative evidence rather than statistically replicated field performance data. Consequently, section-to-section construction variability cannot be separated statistically from the effect of the reinforcement configuration, and confidence intervals or inferential significance tests are not justified. The percentage differences observed between Sections A2 and A3 should therefore be interpreted as descriptive differences under the tested conditions rather than statistically confirmed population effects. The use of common materials, target density, layer thicknesses, loading conditions, instrumentation procedures, and environmental exposure strengthens the internal comparison but does not substitute for replicated test sections. Further testing under controlled temperature conditions and with replicated sections is recommended to generalize the findings. Subgrade soil type and compaction level were not treated as independent variables in the present experimental program. The same clay subgrade source and compaction procedure were maintained in Sections A1–A3 to isolate the effect of geogrid placement location. Therefore, the findings are limited to the tested clay subgrade with a CBR of approximately 5%. Future full-scale studies should investigate different soil types, CBR values, and compaction levels to determine their interaction with geogrid location and pavement performance.

4. Conclusions

- Geogrid reinforcement improved the structural response of the flexible pavement sections under repeated wheel loading compared with the unreinforced control section.
- The unreinforced control section (A1) with the highest rut depth showed the most severe structural response, i.e., the highest vertical stress transmitted to the top of the subgrade and the highest tensile strain at the bottom of the asphalt layer.
- The two reinforced sections reduced permanent surface deformation compared to the control section. However, the section reinforced with geogrid at the top of the granular subbase layer (A3) showed the best rutting performance with a final rut depth of 12.1 mm, compared to 16.5 mm for A2 and 21.5 mm for A1.
- The application of geogrid reinforcement also decreased the vertical stress transmitted to the weak subgrade. The minimum final subgrade stress was observed in section A3 (46.73 kPa) and the second minimum was observed in A2 (48.82 kPa) whereas the maximum value was observed in the control section (56.68 kPa).
- The reinforced sections had lower tensile strain at the bottom of the asphalt binder course than the control section, indicating a better fatigue-related structural response. The lowest final tensile strain among the tested sections was recorded in A3 (154.7 με) followed by A2 (169.5 με) while the highest value was observed in the control section A1 (194.2 με).
- The results show that the geogrid location has a significant effect on the pavement structural performance. Under the current testing conditions, the best overall response in terms of the rutting resistance, subgrade stress reduction and tensile strain reduction was achieved when the geogrid was placed at the top of the granular subbase layer.
- Quantitatively, moving the geogrid from the subgrade–subbase interface in A2 to the top of the subbase in A3 produced an additional 26.7% reduction in final rut depth, 4.3% reduction in final subgrade stress, and 8.7% reduction in final asphalt tensile strain relative to A2. Therefore, the top-of-subbase position provided the best overall structural performance under the tested conditions.

List of Notations and Abbreviations

Notation	Meaning	Notation	Meaning
APT	Accelerated Pavement Testing	DAQ	Data acquisition system
LVDT	Linear variable differential transformer	CBR	California Bearing Ratio
USCS	Unified Soil Classification System	AASHTO	American Association of State Highway and Transportation Officials
HMA	Hot-Mix Asphalt	PP	Polypropylene
MD	Machine direction	TD	Transverse direction
OMC	Optimum moisture content	MDD	Maximum Dry Density
με	Micro strain	A1–A3	Test-section designations

Acknowledgments

The authors gratefully acknowledge the support provided by the College of Civil Engineering, University of Technology, Baghdad, Iraq, during this research. The authors also extend their sincere thanks to Mr. Mustafa Al-Mimar and the colleagues who assisted in the construction of the pavement sections, installation of the instrumentation, and conduct of the tests.

References

[1] Boz I, Coffey GP, Habbouche J, Diefenderfer SD, Ozbulut OE. A critical review of monotonic loading tests to evaluate rutting potential of asphalt mixtures. Construction and Building Materials. 2022;335:127484. https://doi.org/10.1016/j.conbuildmat.2022.127484
[2] Huang YH. Pavement analysis and design. 2nd ed. Pearson; 2004.
[3] Giroud JP, Han J. Design method for geogrid-reinforced unpaved roads. I: Development of design method. Journal of Geotechnical and Geoenvironmental Engineering. 2004;130(8):775-786. https://doi.org/10.1061/(ASCE)1090-0241(2004)130:8(775
[4] Perkins SW. Mechanical response of geosynthetic-reinforced flexible pavements. Geosynthetics International. 1999;6(5):347-382. https://doi.org/10.1680/gein.6.0157
[5] Giroud JP, Han J, Tutumluer E, Dobie MJD. The use of geosynthetics in roads. Geosynthetics International. 2023;30(1):47-80. https://doi.org/10.1680/jgein.21.00046
[6] Alimohammadi H, Zheng J, Schaefer VR, Siekmeier J, Velasquez R. Evaluation of geogrid reinforcement of flexible pavement performance: A review of large-scale laboratory studies. Transportation Geotechnics. 2021;27:100471. https://doi.org/10.1016/j.trgeo.2020.100471
[7] Alimohammadi H, Schaefer VR, Zheng J, Li H. Performance evaluation of geosynthetic reinforced flexible pavement: A review of full-scale field studies. International Journal of Pavement Research and Technology. 2021;14:30-42. https://doi.org/10.1007/s42947-020-0019-y
[8] Abu-Farsakh M, Hanandeh S, Mohammad L, Chen Q. Performance of geosynthetic reinforced/stabilized paved roads built over soft soil under cyclic plate loads. Geotextiles and Geomembranes. 2016;44(6):845-853. https://doi.org/10.1016/j.geotexmem.2016.06.009
[9] Metcalf JB. Application of full-scale accelerated pavement testing. NCHRP Synthesis of Highway Practice 235. Washington, DC: Transportation Research Board, National Research Council; 1996.
[10] Neves J, Freire AC, Qamhia I, Al-Qadi IL, Tutumluer E. Full-scale accelerated pavement testing and instrumentation. In: Advances on testing and experimentation in civil engineering. Springer Tracts in Civil Engineering. Cham: Springer; 2023. p. 163-186. https://doi.org/10.1007/978-3-031-05875-2_7
[11] Chen Q, Hanandeh S, Abu-Farsakh M, Mohammad L. Performance evaluation of full-scale geosynthetic reinforced flexible pavement. Geosynthetics International. 2018;25(1):26-36. https://doi.org/10.1680/jgein.17.00031
[12] Abu-Farsakh MY, Chen Q, Hanandeh S. Accelerated load testing of geosynthetic base reinforced/stabilized unpaved and pavement test sections. Louisiana Transportation Research Center; 2019. Report No. FHWA/LA.18/603.
[13] Barbieri DM, Lou B. Instrumentation and testing for road condition monitoring: A state-of-the-art review. NDT & E International. 2024;146:103161. https://doi.org/10.1016/j.ndteint.2024.103161
[14] Liu Z, Gu X. Performance evaluation of full-scale accelerated pavement using NDT and laboratory tests: A case study in Jiangsu, China. Case Studies in Construction Materials. 2023;18:e02083. https://doi.org/10.1016/j.cscm.2023.e02083
[15] Cho YH, McCullough BF, Weissmann J. Considerations on finite-element method application in pavement structural analysis. Transportation Research Record. 1996;1539:96-101. https://doi.org/10.1177/0361198196153900113
[16] Desai CS. Unified DSC constitutive model for pavement materials with numerical implementation. International Journal of Geomechanics. 2007;7(2):83-101. https://doi.org/10.1061/(ASCE)1532-3641(2007)7:2(83
[17] Saevarsdottir T, Erlingsson S, Carlsson H. Instrumentation and performance modelling of heavy vehicle simulator tests. International Journal of Pavement Engineering. 2016;17(2):148-165. https://doi.org/10.1080/10298436.2014.972957
[18] Baladi GY, Dawson T, Musunuru G, Prohaska M, Thomas K. Pavement performance measures and forecasting and the effects of maintenance and rehabilitation strategy on treatment effectiveness. Federal Highway Administration; 2017. Report No. FHWA-HRT-17-095.
[19] Gu F, Luo X, Luo R, Hajj EY, Lytton RL. A mechanistic-empirical approach to quantify the influence of geogrid on the performance of flexible pavement structures. Transportation Geotechnics. 2017;13:69-80. https://doi.org/10.1016/j.trgeo.2017.08.005

[20] Leonardi G, Suraci F. A 3D-FE model for the rutting prediction in geogrid-reinforced flexible pavements. Sustainability. 2022;14(6):3695. https://doi.org/10.3390/su14063695
[21] Jiang X, Zhang F, Huang B, Titi H, Polaczyk P, Ma Y, et al. Full-scale accelerated testing of geogrid-reinforced inverted pavements. Geotextiles and Geomembranes. 2024;52(4):511-525. https://doi.org/10.1016/j.geotexmem.2024.01.005
[22] Xiao L, Xue J, Xu W. Influence of subgrade spatial variability on strain-alleviating ability of geogrids and rutting life in flexible pavement. Transportation Geotechnics. 2024;49:101368. https://doi.org/10.1016/j.trgeo.2024.101368
[23] Lekarp R, Isacsson U, Dawson A. State of the art. I: Resilient response of unbound aggregates. Journal of Transportation Engineering. 2000;126(1):66-75. https://doi.org/10.1061/(ASCE)0733-947X(2000)126:1(66
[24] Jebur FF, Abduljabbar AS, Fattah MY. Distribution of stresses in reinforced and unreinforced flexible pavement layers under dynamic load. IOP Conference Series: Materials Science and Engineering. 2021;1090:012023. https://doi.org/10.1088/1757-899X/1090/1/012023
[25] Jebur FF, Fattah MY, Abduljabbar AS. Function and application of geogrid in flexible pavement under dynamic load. Engineering and Technology Journal. 2021;39(8):1231-1241. https://doi.org/10.30684/etj.v39i8.1771
[26] Salman ND, Joni HH. Tire contact pressure effects on stress responses of scaled models of geotextile-reinforced flexible pavements over weak subgrade. Engineering and Technology Journal. 2025;43(11):991-1001. https://doi.org/10.30684/etj.2025.164322.2009
[27] Fattah MY, Abd. El-Ghany S, Abdaljabbar AS. Analysis of the performance of flexible pavement under the effect of wheel and thermal loads. Engineering and Technology Journal. 2010;28(18):5782-5802. https://doi.org/10.30684/etj.28.18.14